Metal–organic framework derived hierarchical porous TiO_2 nanopills as a super stable anode for Na-ion batteries

Huan Li[a], Zhiguo Zhang[a], Xiao Huang[a], Tongbin Lan[c], Mingdeng Wei[c], Tingli Ma[a,b,*]

[a] *Graduate School of Life Science and Systems Engineering, Kyushu Institute of Technology, Wakamatsu, Kitakyushu, 808-0196, Japan*

[b] *School of Petroleum and Chemical Engineering , Dalian University of Technology, Liaoning, 124221, China*

[c] *State Key Laboratory of Photocatalysis on Energy and Environment, Fuzhou University, Fuzhou, Fujian 350002, China*

Article history:

Received 26 May 20xx

Revised 9 June 20xx

Accepted 29 June 20xx

Available online

Abstract

Hierarchical porous TiO_2 nanopills were synthesized using a titanium metal-organic framework MIL-125(Ti) as precursor. The as-synthesized TiO_2 nanopills owned a large specific surface area of 102 $m^2\ g^{-1}$ and unique porous structure. Furthermore, the obtained TiO_2 nanopills were applied as anode materials for Na-ion batteries for the first time. The as-synthesized TiO_2 nanopills achieved a high discharge capacity of 196.4 mAh g^{-1} at a current density of 0.1 A g^{-1}. A discharge capacity of 115.9 mAh g^{-1} was obtained at a high current density of 0.5 A g^{-1} and the capacity retention was remained as high as 90% even after 3000 cycles. The excellent electrochemical performance can be attributed to its unique hierarchical porous feature.

Key words: hierarchical porous structure; TiO_2 nanopills; metal–organic framework; Na-ion batteries

*** Corresponding author.** Tel: 093-695-6045; Fax: 093-695-6005; E-mail: tinglima@life.kyutech.ac.jp

1. Introduction

In recent years, Na-ion battery is considered to be a type of highly promising energy storage device, due to the abundance of sodium, the low cost of the production methods, and higher system safety. [1-4] To date, several kinds of materials such as carbonaceous materials, [5-7] sodium alloys, [8-10] sulfides, [11, 12] titanate[13-15] and titanium dioxide have been investigated as the anodes for Na-ion batteries.

Among these materials, titanium dioxide has attracted much attention because of its exceptional stability and abundancy. [16, 17] Its excellent cyclicality and rate capability reported in lithium-ion batteries lead to the further investigation about its sodium storage capability. Xiong et al prepared amorphous TiO_2 nanotube anode and a reversible capacity of 150 mAh g^{-1} was reached in 15 cycles. [18] Anatase TiO_2 nanocrystals was first reported by Xu et al and the discharge capacity of ca. 150 mAh g^{-1} was obtained at a current density of 50 mA g^{-1} for 100 cycles. [19] Three different kinds of TiO_2 including anatase phase, amorphous and rutile phase were compared by Su group. They also demonstrated that the anatase TiO_2 exhibited better sodium storage capability than the other two kinds of TiO_2. [20] However, although TiO_2 owns good cycling stability and reversibility, there is still large space to improve the discharge capacity of this material. In order to refine the electrochemical properties of TiO_2, introducing doping metals and the carbon material additives is a common method reported before. [21-23] Besides, preparing nanosized material to increase the specific area can also be effective for increasing the capacity. [24, 25] It was found that nanosized TiO_2 can exhibit better electrochemical performance than bulk TiO_2.

On the other hand, MOFs (Metal Organic Framework) as a kind of controllable porous functional materials with a large specific surface area, has been explored in various areas in the last few years, including gas storage, [26] adsorptive separation, [27] catalysis, [28] luminescent material, [29] etc. In

addition, MOFs had also been introduced as electrode materials benefiting from their unique porous structure, functional organic linkers and uncoordinated sites. [30-32] However, it was improved that this kind of materials might not be suitable to be directly used as electrode materials for metal ion batteries since partial decomposition would occur during the cycling process. [33, 34] In fact, it had already been reported that MOFs versatile templates and precursors were used to prepare various porous nanomaterials, and further applied in the energy storage field as high-performance electrode materials. A spindle-like porous α-Fe_2O_3 was synthesized by Xu et al. using an iron-based MOF template with a bulk structure composed of clustered Fe_2O_3 nanoparticles, and a discharge capacity as high as 911 mAh g^{-1} was achieved after cycling for 50 times at a rate of 0.2 C. [35] Porous core/shell structured ZnO/$ZnCo_2O_4$/C hybrid was synthesized by Ge group using core/shell ZnCo-MOF precursors as reactant templates and was capable of delivering a specific capacity of 669 mAh g^{-1} after 250 cycles under a current density of 0.5 mA g^{-1} in lithium ion battery. [36]

Therefore, it is significant to combine the advantages of both TiO_2 and MOF materials and synthesize a new kind of electrode material which can not only utilize the large specific surface area and porous structure but also possess excellent stability. In fact, some researchers have already investigated the application of TiO_2 derived from Ti MOF as anode for lithium-ion battery. [37, 38] However, few study about the sodium storage capability of this kind of materials have been reported.

In the present work, the unique structure hierarchical porous TiO_2 nanopills derived from MIL-125(Ti) had been synthesized successfully and used as anode for Na-ion batteries for the first time. This hierarchical porous TiO_2 nanopills exhibits excellent cycling stability and capacity retention as anode for Na-ion batteries. Furthermore, the relationship between the unique 3D structure and the electrochemical properties were also investigated in detail.

2. Experimental

2.1. The synthesis of MIL-125(Ti) and TiO_2

The MIL-125(Ti) was synthesized according to the previous reported method by Wang et al. [39] In a typical process, 0.78 ml of titanium isoproproxide ($Ti(OiPr)_4$, Aldrich, 95%) and 1.3 g of 1,4-benzenedicarboxylic acid (Aldrich, 99%) was dissolved into a mixed solution of 15 ml N,N-dimethylmethanamide (DMF, Sinopharm, 99%) and 1.7 ml methanol (Sinopharm, 99%) under magnetic stirring. After stirring for 1h, the mixed solution was transferred into a 50 ml Teflon-lined stainless autoclave and kept at 150^{o}C for 24 h. After cooling down to room temperature, the precursor was obtained by centrifugation and then washed by menthol and DMF for 3 times. Finally, the sample obtained was dried at 60^{o}C overnight.

To obtain porous TiO_2, the MIL-125(Ti) precursor was calcined at 380 ^{o}C for 4 h with a temperature ramp speed of 5^{o}C/min. The obtained white powder was hierarchical porous anatase TiO_2.

2.2. Characterization of the samples

The samples were characterized by scanning electron microscope (SEM, S5200 instrument), transmission electron microscope (TEM, FEI F20 S-TWIN instrument), X-ray diffraction (XRD, Axis Petro, PANalytical, CoKα, λ=1.79021Å) and automatic specific surface pore distribution measuring apparatus (BET, BELSORP-MR6).

2.3. Measurement of electrochemical properties

The charge and discharge capacities were measured using CR-2025 coin cells, using sodium metal as a counter electrode. The electrode of TiO_2/CB composite were fabricated with the active material TiO_2, conductive material (acetylene black) and binder (PVDF) at a weight ratio of 7:2:1. The

MIL-125(Ti)/CB electrode was also prepared with the same methods for comparison. The electrolyte was 1M $NaClO_4$ in a mixed propylene carbonate (PC) and (EC) solvent (1:1) with 5% fluoroethylene carbonate (FEC) additive. A Land CT2001A battery tester machine was used to measure the electrode activities at room temperature. Charge-discharge measurements were carried out in a potential range of 0.01-3 V versus Na/Na^+ under different current rates. Cyclic voltammetry (CV) measurements were performed on a CHI660C electrochemical workstation at a scan rate of 0.5 mV s^{-1} in the range of 3–0.01 V vs Na/Na^+. The electrochemical impedance measurements were carried out by Zahner IM6 using a 5 mV acoscillation amplitude which was applied over the frequency of 5 MHz to 0.1 Hz frequency ranges. The equivalent circuit was fitted by the Zman 2.0 software of the Zahner IM6 electrochemical workstation.

3. Results and discussion

To study the crystalline phase of the MIL-125(Ti) precursor and hierarchical porous TiO_2, XRD patterns of the two samples are displayed in Fig. 1 and Fig. S1, respectively. Fig. S1 showed that the XRD pattern of MIL-125(Ti) was in good agreement with the previous report. [39] The sharp and strong peaks indicated the large size of MIL-125(Ti). After calcined at 380°C, all the peaks in Fig. 1 could be indexed to anatase TiO_2 (JCPDs-01-078-2486) with no any peaks coming from MIL-125(Ti). The major diffraction peaks appeared at 2θ values of 25°, 37° and 47° could be indexed to (101), (004) and (200) face of anatase TiO_2, respectively.

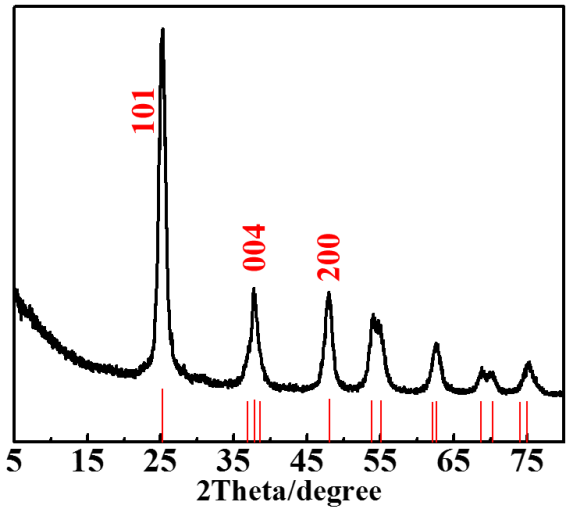

Figure 1 XRD pattern of hierarchically porous TiO_2.

Fig. 2 showed the SEM images of MIL-125(Ti) and hierarchical porous TiO_2. It can be seen from Fig. 2a-b that a large number of circles in microsize scale for the MIL-125(Ti) precursor with a uniform diameter of ca. 1 μm. After calcined at 380°C, the anatase TiO_2 derived from MIL-125(Ti) could remain the integrated morphology of circles and exhibited a hierarchical porous structure composed of nanoparticles, which was depicted in Fig. 2c-d. However, the particle size of the as-synthesized TiO_2 crystal had been reduced to ca. 500-700 nm due to the loss of C and H atoms during the calcinations process.

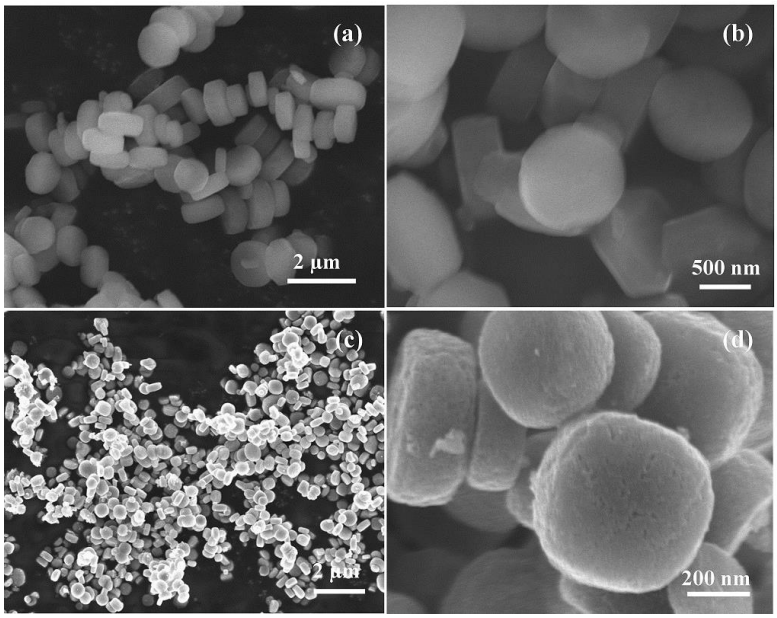

Figure 2 SEM images of MIL-125(Ti) precursor (a-b) and the hierarchically porous TiO_2 (c-d) derived from MIL-125(Ti).

Moreover, the detailed analysis of TiO_2 sample and MIL-125(Ti) was investigated by TEM and SAED measurements. The HRTEM image in Fig. 3a confirmed that the MIL-125(Ti) was made of bulk with a diameter of ca. 1 μm. Fig. 3b presented the basic morphology of nanopills hadn't been changed for the TiO_2 sample after calcined. However, the anatase TiO_2 derived from MIL-125(Ti) cubic changed to a porous structure and was composed of nanoparticles smaller than 10 nm, as depicted in Fig. 3b. As shown in Fig. 3c, a lattice fringe of 0.352 nm which corresponds to (101) face of TiO_2 can be observed. The different direction of lattice fringe proved the existence of nanoparticles as well. Besides, the SAED pattern in Fig. 3d delivered some typical crystal planes of anatase TiO_2, which was consistent with the XRD pattern of anatase TiO_2.

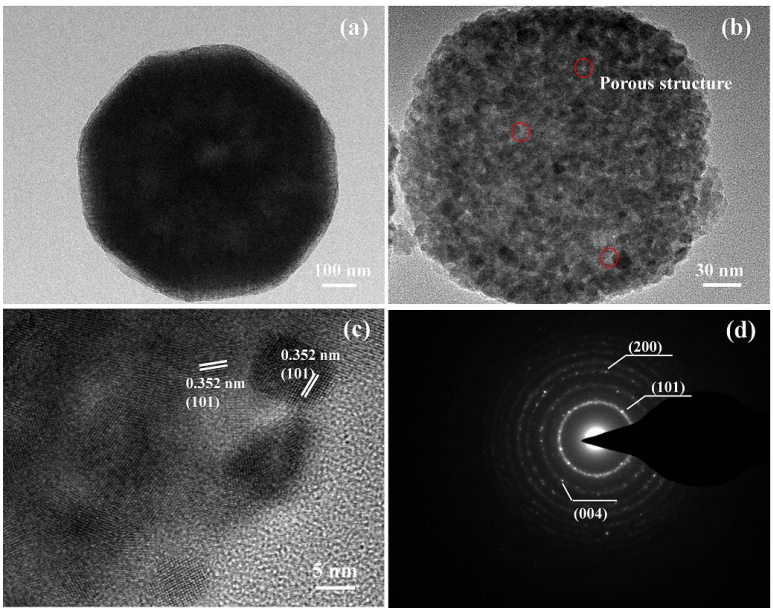

Figure 3 (a) TEM image of MIL-125(Ti) precursor, (b) TEM image, (c) HRTEM image and (d) SAED pattern of the hierarchically porous TiO_2 derived from MIL-125(Ti).

In order to further investigate the homogeneity and hierarchical structure of hierarchical porous TiO_2 nanopills, the particle size distribution of sample was shown in Fig. 4. As depicted in Fig. 4, the particle size of hierarchical porous TiO_2 nanopills ranges from 400-600 nm, and an average particle size of 520 nm could be obtained, which was in good agreement with the SEM and TEM results. In addition, the particle size distribution of MIL-125(Ti) precursor was also shown in Fig.S2 as a comparison. As depicted in Fig. S2, the particle size of MIL-125(Ti) precursor ranges from 0.88-1.52 μm, and have an average size of 1.18 μm.

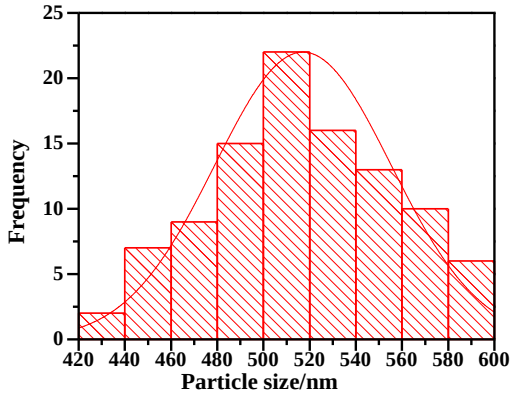

Figure 4 Size distribution of hierarchically porous TiO_2.

Nitrogen adsorption-desorption isotherm characterization was used to further investigate the pore size distribution and specific surface area of the hierarchical porous TiO_2. As shown in Fig. 5, the hierarchical porous TiO_2 showed a specific surface area as high as 102 $m^2 g^{-1}$. The pore diameter distribution result in Fig. 5b showed that the hierarchical TiO_2 nanopills had a mean pore size value of ca. 11 nm, in agreement with the results of TEM measurement, indicating the existence of mesopores. Such a large BET surface area and complex porous structure of hierarchical porous TiO_2 could be propitious to the diffusion of Na ions and electrolyte. The MIL-125(Ti) was also tested with the same method as a comparison, as depicted in Fig. S3. The MIL-125(Ti) had a large specific surface area of 1167 $m^2 g^{-1}$.

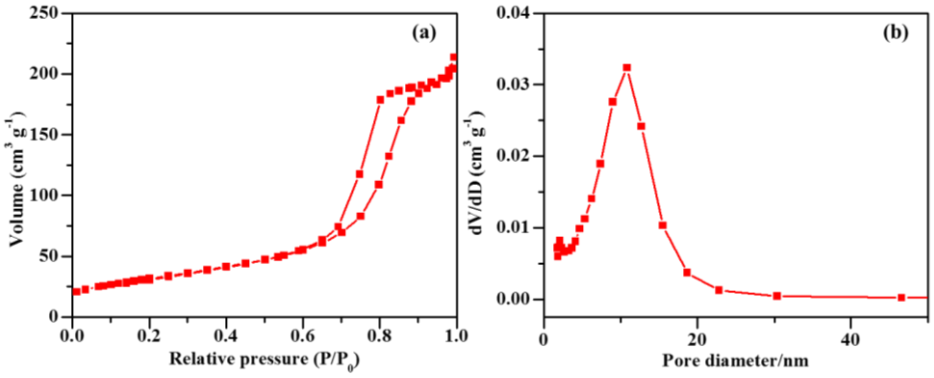

Figure 5 (a) N_2 adsorption-desorption isotherms and (b) pore size distributions from the adsorption branch through the BJH method of hierarchically porous TiO_2 nanopills.

CV curves of the hierarchical porous TiO_2 anode are shown in Fig. 6a. For the initial cycle, a redox peak at 0.87 V could be observed, which disappeared in the following cycles; this might be ascribed to the decomposition of electrolyte, the formation of solid electrolyte interphase (SEI) film and some irreversible structure change of the active materials. [40-42] Upon subsequent cycling, an oxidation peak at 0.75V and a redox peak at 0.5V could be observed which could be assigned to the reversible reduction of Ti^{4+}/Ti^{3+}. Besides, the oxidation and redox peaks for each cycle did not change, illustrating the reversibility of sodium ions storage process in the electrode.

Fig. 6b shows the discharge-charge profiles of TiO_2/CB electrode at a current density of 0.1 A g^{-1} in a

voltage range of 0.01-3V for 1st, 2nd and 50th cycles, respectively. An initial discharge capacity of 516.2 mA h g^{-1} could be obtained due to the formation of solid electrolyte interphase (SEI) film just corresponding to the result of CV curves. Besides, it exhibited a discharge capacity of 196.4 and 164.3 mA h g^{-1} for the 2nd and 50th cycles, respectively, which illustrated the excellent cycling stability of the hierarchical porous TiO_2 anode. As a comparison, the MIL-125(Ti) was tested at the same current density. As depicted in Fig. S4, a discharge capacity of 115.9 and 71.6 mA h g^{-1} for the 2nd and 10th cycles at a current density of 0.05 A g^{-1} were obtained, respectively. This result demonstrated that MIL-125(Ti) cannot exhibit good electrochemical performance for Na-ion batteries, because of the possibly decomposition during cycling process.

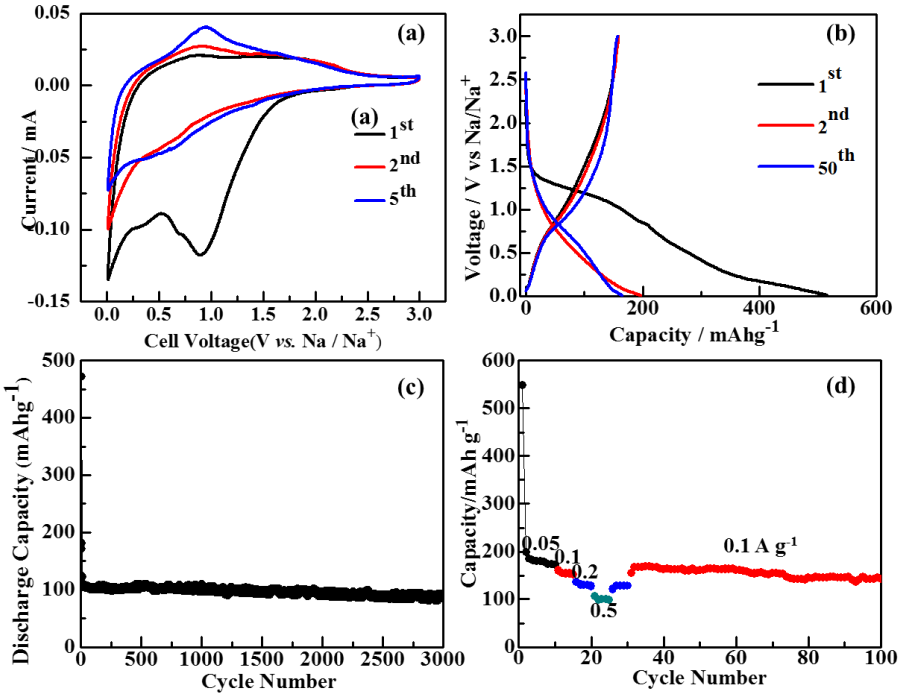

Figure 6 (a) CV curves for the 1st, 2nd and 5th cycles at a scan rate of 0.5 mV s^{-1}, (b) charge-discharge profiles for the 1st, 2nd and 50th cycles at a current density of 0.1 A g^{-1}, (c) cycling performance at a current density of 0.5 A g^{-1} and (d) rate performance of the hierarchically porous TiO_2 electrode.

The hierarchical porous TiO_2 anode was also tested at a current density of 0.5 A g^{-1}, as shown in Fig. 6c. The cell was cycled at a relative small current density of 0.05 A g^{-1} for the initial three cycles for the

activation of the electrode. A high discharge capacity of 100 mA h g^{-1} could be remained even after 3000 cycles. Moreover, the capacity retention could be remained as high as 90%, indicating the excellent cycling stability of this material. In addition, the cycling stability of hierarchical porous TiO_2 nanopills were better than most previous reports. [18, 19, 24, 25] Fig. 6d presents the rate capability of hierarchical porous TiO_2 from 0.05 to 0.5 A g^{-1}. The reversible discharge capacities of hierarchical porous TiO_2 could reach 170 mAh g^{-1} at 0.05 A g^{-1} and 110 mAh g^{-1} at a relatively high rate of 0.5 A g^{-1}, respectively. Besides, a specific capacity of 160 mA h g^{-1} could be achieved when the current density was returned to an initial value of 0.1 A g^{-1} after 30 cycles, and could continually remain for 100 cycles, which indicated this material owns a high reversibility. In addition, the SEM and TEM images of the TiO_2/CB electrode after cycling were offered in Fig.S6 and S7 to further assume the structural stability, respectively.

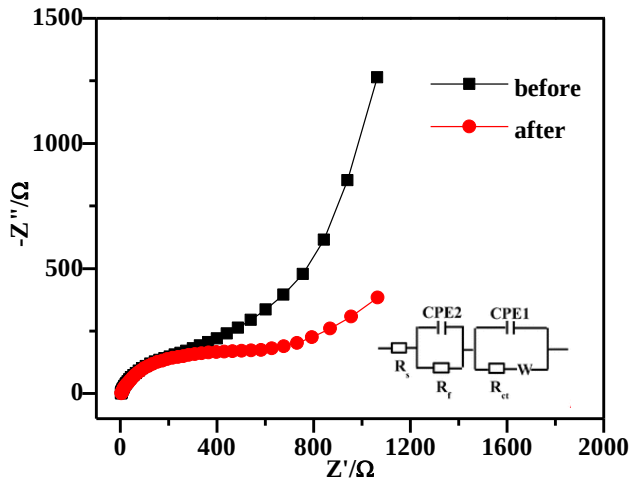

Figure 7 EIS of the hierarchically porous TiO_2 electrode before and after 2000 cycles.

Table 1 Impedance parameters calculated from an equivalent circuit model.

Samples	Rs(Ω)	Rct(Ω)
Before	3.22	31.27

After	3.78	16.54

Fig. 7 shows the EIS plots of a hierarchical porous TiO_2/CB composite electrode before and after cycling for 2000 cycles at 0.5 A g^{-1}. It can be seen that the plots are all composed of a semicircle at high frequencies which were related to the Ohmic resistance and charge transfer resistance, and a short inclined line in low frequency regions which was due to the ion diffusion within the anode. [29]The semicircle for the hierarchical porous TiO_2 electrode before cycling was a little smaller than that of the sample after cycling, indicating that the charge transfer resistance increased after 2000 cycles. In order to further analysis this phenomenon, the impedance plots of the TiO_2/CB electrode before and after cycling were both fitted by using an equivalent circuit model, as shown in the inset of Fig. 7. The equivalent circuit model included the electrolyte resistance R_s, the SEI resistance R_f, the charge-transfer resistance R_{ct}, the Warburg impedance (W) related to the diffusion rate of Na ions into the bulk of the electrode and two constant phase elements (CPE1 and CPE2) which correspond to the charge-transfer resistance and interfacial resistance, respectively. From the EIS fitting values shown in Table. 1, R_s values increased slightly from 3.22 Ω to 3.78 Ω after cycling for 2000 cycles. However, the charge transfer resistance R_{ct} decreased after 2000 cycles, which could be due to the reduction of the nanocomposite into their corresponding metals during the irreversible reactions. This phenomenon also appeared in similar metal oxide electrode materials in lithium ion batteries. [43, 44]

In this study, hierarchical porous TiO_2 derived from MIL-125(Ti) exhibited excellent electrochemical performance which is considered to be due to its unique intrinsic characteristics including the following aspects, as illustrated in Fig. 8. Firstly, the as prepared TiO_2 retained the basic framework of MIL-125(Ti) which could benefit for the diffusion of electrolyte. Secondly, the porous structure could be

advantageous for promoting electrode/electrolyte wettability and increasing ion absorption sites by generating extrinsic defects. Thirdly, this material has a large specific surface area which could effectively increase the contact between electrolyte and active mass, further improving the storage capabilities for Na-ions. As mentioned above, these advantages lead to the excellent electrochemical properties of hierarchical porous TiO_2 nanopills.

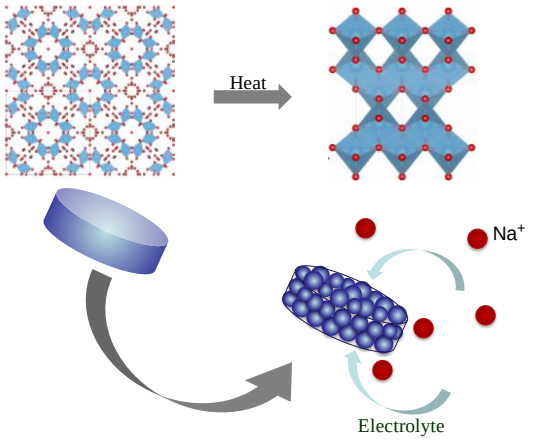

Figure 8 The diffusion and storage of Na^+ ions in the hierarchical porous TiO_2 nanopills.

Conclusions

In summary, the unique hierarchical porous TiO_2 nanopills derived from MIL-125(Ti) had been synthesized successfully by hydrothermal method and the following calcination. For the first time, this material was used as the anode material for Na-ion batteries. The materials exhibited high reversible capacity and excellent rate capability. We obtained a high specific capacity of 196.4 and 115.9 mA h g^{-1} at 0.1 A g^{-1} for the 2^{nd} cycle and 0.5 A g^{-1}, respectively. Furthermore, it still remained a capacity of 100 mA h g^{-1} and a capacity retention as high as 90% even after cycling for 3000 times at a high current density of 0.5 A g^{-1}. Therefore, this kind of anode material can be a promising candidate for the high-capacity rechargeable Na-ion batteries. Our results indicate this kind of material derived from MOF can be applied as the potential electrodes for the other energy storage devices.

Acknowledgments

This work was supported by JSPS KAKENHI Grant Number 15K00597 and Takahashi Industrial and Economic Research Foundation Japan.

References:

[1] D. A. Stevens and J. R. Dahn, Electrochem. Soc. 147 (2000) 1271.

[2] M. D. Slater, D. Kim, E. Lee, M. M. Doeff and C. S. Johnson, Adv. Funct. Mater. 23 (2013) 947.

[3] H. Pan, Y. Hu and L. Chen, Energy & Environ. Sci. 6 (2013) 2338-2360.

[4] C. Nithya and S. Gopukumar, Wiley Interdisciplinary Reviews: Energy and Environment 4 (2015) 253-278.

[5] S. Komaba, W. Murata, T. Ishikawa, N. Yabuuchi. T. Ozeki, T. Nakayama, A. Ogata, K. Gotoh and K. Fujiwara, Adv. Funct. Mater. 21 (2011) 3859-3867.

[6] H. Hou, C. E. Banks, M. Jing, Y. Zhang and X. Ji, Adv. Mater. 27 (2015) 7861-7866.

[7] Y. Li, Y. Hu, M. Titirici, L. Chen and X. Huang, Adv. Energy Mater. (2016).

[8] P. R. Abel, M. G. Fields, A. Heller and C. B. Mullins, ACS Appl. Mater. Interfaces 6 (2014) 15860-15867.

[9] Zhao Y and Manthiram A, Chem.Mater. 27 (2015) 3096-3101.

[10] C. Yue, Y. Yu, S. Sun, X. He, B. Chen, W. Lin, B. Xu, M. Zheng, S. Wu, J. Li, J. Kang and L. Lin, Adv. Funct. Mater. 25 (2015) 1386-1392.

[11] C. Zhu, P. Kopold, W. Li, P. A. Aken, J. Maier and Y. Yu. Advanced Science 2 (2015) 1500200.

[12] S. Peng, X. Han, L. Li, Z. Zhu, F. Cheng, M. Srinivansan, S. Adams and S. Ramakrishna, Small 12 (2016).

[13] H. Li, H. Fei, X. Liu, J. Yang and M. Wei, Chem. Commun. 51 (2015) 9298-9300.

[14] Q. Zhang, Y. Guo, K. Guo, T. Zhai and H. Li, Chem. Commun. 52 (2016) 6229-6232.

[15] Y. Zhang, H. Hou, X. Yang, J. Chen, M. Jing, Z. Wu, X. Jia and X. Ji, J. Power Sources 305 (2016) 200-208.

[16] Z. Hong, M. Wei, T. Lan, L. Jiang and G. Cao, Energy Environ. Sci. 5 (2012) 5408–5413.

[17] Z. Hong and M. Wei, J. Mater. Chem. A 1 (2013) 4403–4414.

[18] H. Xiong, M. D. Slater, M. Balasubramanian, C.S. Johnson and T. Rajh, J. Phys. Chem. Lett 2 (2011) 2560-2565.

[19] Y. Xu, E. M. Lotfabad, H. Wang, B. Farbod, Z. Xu, A. Kohandehghan and D. Mitlin, Chem. Commun. 49 (2013) 8973-8975.

[20] D. Su, S. Dou and G. Wang, Chem. Mater. 27 (2015) 6022-6029.

[21] C. Ding, T. Nohira, R. Hagiwara, J. Mater. Chem. A 3 (2015) 20767-20771.

[22] S. M. Oh, J. Y. Hwang, C. S. Yoon, J. Lu, K. Amine, I. Belharouak and Y. K. Sun, ACS Appl. Mater. Interfaces 6 (2014) 11295-11301.

[23] H. Usui, S. Yoshioka, K. Wasada, M. Shimizu and H. Sakaguchi, ACS Appl. Mater. Interfaces 7 (2015) 6567-6573.

[24] K. Kim, G. Ali, K. Y. Chung, C. S. Yoon, H. Yashiro, Y. Sun, J. Lu, K. Amine and S. Myung, Nano Lett. 14 (2014) 416-422.

[25] J. P. Huang, D. D. Yuan, H. Z. Zhang, Y. L. Cao, G. R. Li, H. X. Yang and X. P. Gao, RSC Advances 3 (2013) 12593.

[26] T. A. Makal, J.-R. Li, W. Lu and H. C. Zhou, Chem. Soc. Rev. 41 (2012) 7761–7779.

[27] R. Dawson, E. St¨ockel, J. R. Holst, D. J. Adams and A. I. Cooper, Energy Environ. Sci. 4 (2011) 4239–4245.

[28] R. Q. Zou, H. Sakurai, S. Han, R. Q. Zhong and Q. Xu, J. Am. Chem. Soc. 129 (2007) 8402–8403.

[29] L. Chen, K. Tan, Y. Q. Lan, S. L. Li, K. Z. Shao and Z. M. Su, Chem. Commun. 48 (2012) 5919–5921.

[30] A. Morozan and F. Jaouen, Energy Environ. Sci. 5 (2012) 9269–9290.

[31] C. Y. Cheng, S. J. Fu, C. J. Yang, W. H. Chen, K. J. Lin, G. H. Lee and Y. Wang, Angew. Chem., Int. Ed. 42 (2003) 1937–1940.

[32] L. W. Huang, C. J. Yang and K. J. Lin, Chem.–Eur. J. 8 (2002) 396–400.

[33] X. Li, F. Cheng, S. Zhang and J. Chen, J. Power Sources 160 (2006) 542–547.

[34] G. F´erey, F. Millange, M. Morcrette, C. Serre, M. L. Doublet, J. M. Greneche and J. M. Tarascon, Angew. Chem., Int. Ed. 46 (2007) 3259–3263.

[35] X. Xu, R. Cao, S. Jeong and J. Cho, Nano Lett. 12 (2012) 4988-4991.

[36] X. Ge, Z. Q. Li, C. X. W and L. W. Yin, ACS Appl. Mater. Interfaces 7 (2015) 26633–26642.

[37] Z. Xiu, M. H. Alfaruqi, J. Gim, J. Song, S. Kim, T. V. Thi, P. T. Duong, J. P. Baboo, V. Mathew and J. Kim, Chem. Commun., 51 (2015) 12274-12277.

[38] P. Wang, J. W. Lang, D. X. Liu and X. B. Yan, Chem. Commun. 51 (2015) 11370-11373.

[39] S. N. Kim, J. Kim, H. Y. Kim, H. Y. Cho and W. S. Ahn, Catalysis today, 204 (2013) 85-93.

[40] Y.G. Guo, J. S. Hu, L. J. Wan, Adv. Mater. 20 (2008) 2878-2887.

[41] X. Yang, C. Wang, Y. Yang, Y. Zhang, X. Jia, J. Chen, X. Ji, J. Mater. Chem. A 3 (2015) 8800-8807.

[42] L. Wu, D. Bresser, D. Buchholz, G. A. Giffin, C. R. Castro, A. Ochel, S. Passerini, Adv. Energy Mater. 5 (2015) 1401142.

[43] J. Luo, J. Liu, Z. Zeng, C. Ng, L. Ma, H. Zhang, J. Lin, Z. Shen and H. Fan. Nano Lett. 13(2013) 6136-6143.

[44] F. Lu, Q. Chen, Y. Wang, Y. Wu, P. Wei and X. Kuang. RSC Adv. 6(2016) 24366-24372.